

Parameter-efficient Fine-tuning in Hyperspherical Space for Open-vocabulary Semantic Segmentation

Zelin Peng¹ Zhengqin Xu¹ Zhilin Zeng¹ Yaoming Wang² Wei Shen¹(✉)

¹Shanghai Jiao Tong University

²Huawei Inc.

{zelin.peng, fate311, bernardeschi, wang.yaoming, wei.shen}@sjtu.edu.cn;

Abstract

Open-vocabulary semantic segmentation seeks to label each pixel in an image with arbitrary text descriptions. Vision-language foundation models, especially CLIP, have recently emerged as powerful tools for acquiring open-vocabulary capabilities. However, fine-tuning CLIP to equip it with pixel-level prediction ability often suffers three issues: 1) high computational cost, 2) misalignment between the two inherent modalities of CLIP, and 3) degraded generalization ability on unseen categories. To address these issues, we propose H-CLIP, a symmetrical parameter-efficient fine-tuning (PEFT) strategy conducted in hyperspherical space for both of the two CLIP modalities. Specifically, the PEFT strategy is achieved by a series of efficient block-diagonal learnable transformation matrices and a dual cross-relation communication module among all learnable matrices. Since the PEFT strategy is conducted symmetrically to the two CLIP modalities, the misalignment between them is mitigated. Furthermore, we apply an additional constraint to PEFT on the CLIP text encoder according to the hyperspherical energy principle, i.e., minimizing hyperspherical energy during fine-tuning preserves the intrinsic structure of the original parameter space, to prevent the destruction of the generalization ability offered by the CLIP text encoder. Extensive evaluations across various benchmarks show that H-CLIP achieves new SOTA open-vocabulary semantic segmentation results while only requiring updating approximately 4% of the total parameters of CLIP.

1. Introduction

The aim of open-vocabulary semantic segmentation is to create a segmentation model capable of labeling each pixel in an image with categories that are not limited to a specific closed set according to text descriptions. Vision-language founda-

tion models [5, 10, 11, 13, 18, 20, 22, 27–30, 36, 41, 46, 48], especially CLIP [41], are often utilized to endow open-vocabulary recognition capabilities. Consequently, open-vocabulary semantic segmentation essentially boil down to transferring these vision-language foundation models, originally trained with image-level supervision, to perform pixel-level predictions.

To this end, current methods [7, 52, 55, 56] typically fine-tune CLIP on a benchmark dataset with segmentation annotations, i.e., COCO [2], to equip it with the segmentation ability. However, this often leads to three main issues. First, fine-tuning CLIP on limited categories would affect its generalization ability, resulting in significant performance degradation on unseen categories. Second, current fine-tuning methods for open-vocabulary segmentation are usually asymmetrical [26, 52, 55], i.e., typically freezing CLIP’s text encoder and fine-tuning its image encoder. This strategy inevitably causes a potential obstacle: misalignment. More specifically, the misalignment arises from different alignment granularities. The text encoder maintains image-to-text alignment, while the image encoder shifts from image-to-text to pixel-to-text alignment. Due to these different alignment goals, the optimization process is largely impeded, leading to sub-optimal performance. Third, although remarkable performance gains, these approaches often rely on computationally extensive full fine-tuning, which raises concerns about scalability and affordability.

To address these issues, we propose a symmetric parameter-efficient fine-tuning strategy for CLIP, dubbed H-CLIP. First, to preserve CLIP’s generalization ability, we are inspired by the hyperspherical energy principle [35, 40], which suggests that maintaining the same hyperspherical energy during fine-tuning preserves the intrinsic structure, i.e., generalization capability. Therefore, H-CLIP is fine-tuned in hyperspherical space, incorporating orthogonal constraints in the learnable matrices of CLIP’s text encoder. These orthogonal transformations are realized in a block-diagonal form to efficiently maintain the invariance of hyperspherical energy during fine-tuning. Second, by fine-tuning both

✉ Corresponding Author: wei.shen@sjtu.edu.cn

modalities of CLIP with a comparable number of parameters, we largely mitigate the misalignment. Then, to further enhance alignment between different modalities of CLIP, we introduce a dual cross-relation communication (DCRC) module to explicitly encourage cross-modal and cross-layer communications within all learnable matrices. Notably, DCRC encourages the alignment problem with minimal overhead. Consequently, H-CLIP can adapt CLIP for open vocabulary semantic segmentation with only a small number of introduced learnable parameters.

Extensive results demonstrate that H-CLIP achieves new state-of-the-art open-vocabulary semantic segmentation results across three benchmarks by fine-tuning CLIP with approximately 4% of the total parameters of CLIP.

2. Related Work

2.1. Open-vocabulary Semantic Segmentation

Prior open-vocabulary semantic segmentation works typically perform this task through leveraging CLIP [41]. initial efforts like [60] directly fine-tune CLIP on mainstream segmentation datasets, e.g., COCO [2]. However, they claim that fine-tuning CLIP’s encoder significantly reduces its ability to generalize to unseen classes. To address this issue, some methods [8, 15, 53, 54] swing to the opposite extreme, fine-tuning an additional mask generator [6] for segmentation while keeping CLIP frozen to maintain generalization-oriented recognition. However, this frozen parameter space lacks segmentation awareness, resulting in a misalignment between regions and text descriptions [32]. Other studies [7, 55, 56] propose an advanced solution that fine-tunes only selected parameters, e.g., certain layers of CLIP, to enable pixel-level predictions while keeping most of CLIP’s parameters fixed, thus minimizing losing of generalization. Although the advantages are remarkable, these methods often work with a very small learning rate, implicitly encouraging a small deviation from the pre-trained CLIP, limiting the segmentation performance. In a nutshell, the trade-off between preserving CLIP’s generalization and learning segmentation knowledge persists, hindering the final performance. Based on the paradigm of existing fine-tuning-based methods, our method explores a better trade-off from a fresh viewpoint: hyperspherical space.

2.2. Large-scale Model Fine-tuning

Along with the improvement of large-scale foundation models [24, 28, 29, 36, 42–44, 57, 64], e.g., segment anything model [24], numerous fine-tuning works [4, 14, 34, 38, 39, 50, 58, 61, 62, 65] are proposed to adapt these models to various downstream scenarios. The core of these approaches lies in updating only limited parameters to capture the specific characteristics of different scenarios, while keeping most parameters fixed to maintain generalization. In contrast, fine-

tuning CLIP for open-vocabulary semantic segmentation often meets a dilemma. On the one hand, limited parameters typically fall short in facilitating the transition from a classification model, i.e., CLIP, to a segmentation task. On the other hand, directly increasing the number of trainable parameters risks undermining CLIP’s ability to generalize to unseen classes, as experimented in CAT-Seg [7]. Most methods [52, 56] solve this issue by simply freezing CLIP’s text encoder and fine-tuning its image encoder, inevitably causing misalignment between the two modalities of CLIP. In this paper, we shed light on how to preserve generalization in a symmetric parameter-efficient fine-tuning manner and strive to explore an appropriate fine-tuning method for open-vocabulary semantic segmentation.

3. Preliminaries

3.1. Hyperspherical Energy

Existing fine-tuning methods implicitly assume that a smaller Euclidean distance between the fine-tuned model and the pre-trained model indicates better preservation of the pre-trained ability. However, Euclidean distance is insufficient to fully capture the degree of semantic preservation. Inspired by the Thomson problem [47], which seeks to determine the minimum electrostatic potential energy configuration of N mutually-repelling electrons on the surface of a unit sphere, we adopt the *Hyperspherical Energy* to characterize the diversity of the model.

The hyperspherical energy function of a fully connected layer \mathbf{W} is defined as:

$$\text{HE}(\mathbf{W}) := \sum_{i \neq j} \|\hat{\mathbf{w}}_i - \hat{\mathbf{w}}_j\|^{-1}$$

where $\hat{\mathbf{w}}_i := \mathbf{w}_i / \|\mathbf{w}_i\|$ denotes the i -th normalized neuron. The power of the model representation can be characterized by the hyperspherical energy of its neurons. Higher energy implies greater redundancy, while lower energy indicates that the neurons of the model are more diverse.

To ensure that the generalization is not destroyed during fine-tuning, we hypothesize that a good fine-tuning model should minimize the difference in hyperspherical energy compared to the pre-trained model:

$$\begin{aligned} & \min_{\mathbf{W}} \|\text{HE}(\mathbf{W}) - \text{HE}(\mathbf{W}^0)\| \\ & \Leftrightarrow \min_{\mathbf{W}} \left\| \sum_{i \neq j} \|\hat{\mathbf{w}}_i - \hat{\mathbf{w}}_j\|^{-1} - \sum_{i \neq j} \|\hat{\mathbf{w}}_i^0 - \hat{\mathbf{w}}_j^0\|^{-1} \right\|. \end{aligned} \quad (1)$$

It is evident that the attainable minimum is zero for Eq. (1). In this case, the hyperspherical energy satisfies an invariance property: applying the same orthogonal transformation to all neurons preserves pairwise hyperspherical similarity. Consequently, the minimum of zero can be achieved as long

as \mathbf{W} and \mathbf{W}^0 differ only by a rotation or reflection, i.e., $\mathbf{W} = \mathbf{R}\mathbf{W}^0$ where $\mathbf{R} \in \mathbb{R}^{d \times d}$ is an orthogonal matrix (with determinant 1 for rotation or -1 for reflection).

3.2. Notation of Tensor Product

In this section, we introduce the fundamental concept to achieve dual cross relation communication (Sec. 4.3): tensor product. A p -order tensor is indexed by p indices and can be represented as a multidimensional array of data. Formally, a p -order tensor \mathcal{A} can be written as $\mathcal{A} = (a_{i_1, i_2, \dots, i_p}) \in \mathbb{R}^{n_1 \times n_2 \times \dots \times n_p}$. Slices of a tensor are matrices defined from the tensor by holding all but two indices constant. For a 3-order tensor, $\mathcal{A}(:, :, k)$ corresponds the k^{th} frontal slice. For p -order tensors, matrix slices of p -order tensors can be referenced using linear indexing by reshaping the tensor into an $n_1 \times n_2 \times n_3 \times \dots \times n_p$ 3-order tensor and referring to the k^{th} frontal slice as $\mathcal{A}(:, :, k)$. $\mathcal{A}_i \in \mathbb{R}^{n_1 \times n_2 \times \dots \times n_{p-1}}$ for $i = 1, \dots, n_p$ denotes the $(p-1)$ -order tensor created by holding the p^{th} index of \mathcal{A} fixed at i . It is possible to create a tensor in a block circulant pattern, where each block is a tensor of $(p-1)$ -order:

$$\text{circ}(\mathcal{A}) = \begin{bmatrix} \mathcal{A}_1 & \mathcal{A}_{n_p} & \mathcal{A}_{n_p-1} & \dots & \mathcal{A}_2 \\ \mathcal{A}_2 & \mathcal{A}_1 & \mathcal{A}_{n_p} & \dots & \mathcal{A}_3 \\ \vdots & \vdots & \vdots & \ddots & \vdots \\ \mathcal{A}_{n_p} & \mathcal{A}_{n_p-1} & \mathcal{A}_{n_p-2} & \dots & \mathcal{A}_1 \end{bmatrix}, \quad (2)$$

where $\text{circ}(\cdot)$ creates a block circulant tensor and the size of $\text{circ}(\mathcal{A})$ is $(n_1 n_p \times n_2 n_p \times \dots \times n_{p-2} n_p \times n_{p-1})$. Define $\text{unfold}(\cdot)$ to take an $n_1 \times \dots \times n_p$ tensor \mathcal{A} and return an $n_1 n_p \times n_2 \times \dots \times n_{p-1}$ block tensor in the following way:

$$\text{unfold}(\mathcal{A}) = [\mathcal{A}_1 \ \mathcal{A}_2 \ \dots \ \mathcal{A}_{n_p}]^T. \quad (3)$$

The operation that takes unfold back to tensor form is the “fold” command. Specially, $\text{fold}(\cdot, n_p)$ takes an $n_1 n_p \times n_2 \times \dots \times n_{p-1}$ block tensor and returns an $n_1 \times \dots \times n_p$ tensor, defined as:

$$\text{fold}(\text{unfold}(\mathcal{A}), n_p) = \mathcal{A}. \quad (4)$$

4. Methodology

4.1. Overview of H-CLIP

Fig. 1 illustrates the proposed H-CLIP framework, which is based on two core components: (1) POP updates the pre-trained parameter space of CLIP using a series of block-diagonal transformation matrices. According to analysis in Sec. 1, each parameter matrix in CLIP’s text encoder is orthogonal to preserve generalization. (2) DCRC incorporates cross-modal and cross-layer communication within all tunable matrices, facilitating alignment between different modalities.

4.2. Partial Orthogonal Parameterization

The core idea of partial orthogonal parametrization (POP) is to introduce the concept of hyperspherical space for fine-tuning CLIP. In this hyperspherical space, we fine-tune CLIP’s text encoder under an orthogonality design principle from OFT [40] to preserve the hyperspherical energy of the pre-trained parameter space. Similarly, we use Cayley parameterization [3] to ensure a tunable matrix \mathbf{R} is strictly orthogonal, formally as:

$$\mathbf{R} = (\mathbf{I} + \mathbf{Q})(\mathbf{I} - \mathbf{Q})^{-1}, \quad (5)$$

where \mathbf{Q} is skew-symmetric. Guided by the observation in [26, 32] that CLIP’s generalization ability is primarily preserved in its text encoder, we impose an orthogonality constraint on the tunable matrices within CLIP’s text encoder during fine-tuning, which is defined as:

$$\mathbf{R}^\top \mathbf{R} = \mathbf{R} \mathbf{R}^\top = \mathbf{I}, \quad (6)$$

where \mathbf{I} is an identity matrix. Considering the relatively large dimension d of the pre-trained matrix, for better efficiency, we introduce a block-diagonal structure by parameterizing \mathbf{R} with b blocks, formally as:

$$\mathbf{R} = \text{diag}(\mathbf{R}_1, \mathbf{R}_2, \dots, \mathbf{R}_i, \dots, \mathbf{R}_b) = \begin{bmatrix} \mathbf{R}_1 & & \\ & \ddots & \\ & & \mathbf{R}_b \end{bmatrix}, \quad (7)$$

where $\mathbf{R}_i \in \mathbb{R}^{d/b \times d/b}$. Specifically, denote $\mathcal{R}^V = \{\mathbf{R}_{v1}, \dots, \mathbf{R}_{v\ell}, \dots, \mathbf{R}_{vL}\}$ and $\mathcal{R}^E = \{\mathbf{R}_{e1}, \dots, \mathbf{R}_{e\ell}, \dots, \mathbf{R}_{eL}\}$ as the sets of block-diagonal matrices in CLIP’s image encoder and text encoder, respectively, where L is its number of Transformer layers, $\mathbf{R}_{v\ell} \in \mathbb{R}^{d_v \times d_v}$, and $\mathbf{R}_{e\ell} \in \mathbb{R}^{d_e \times d_e}$. In practice, the dimensions of the tunable matrix $\mathbf{R}_{vi} \in \mathbb{R}^{d_v \times d_v}$ and $\mathbf{R}_{ei} \in \mathbb{R}^{d_e \times d_e}$ are often not equal, e.g., $d_v = 768$ and $d_v = 512$ for ViT/16 version of CLIP. Considering that the dimension of each individual slice in a higher-order tensor must be consistent according to the tensor theorem, we use a block diagonal structure to align the matrix dimensions between the two modalities, and thus, it cannot be discarded. For notation simplicity, we set $d_v = d_e = d$.

4.3. Dual Cross Relation Communication

Although in POP, we relax the orthogonal constraint for CLIP’s image encoder to learn segmentation capability, each layer of the image encoder still incorporates a limited number of parameters, which largely restricts the flexibility of the projection adjustment due to the limitation of Hidden Markov Chain along layers [25, 38, 49]. To address this limitation, one might consider fully fine-tuning instead of

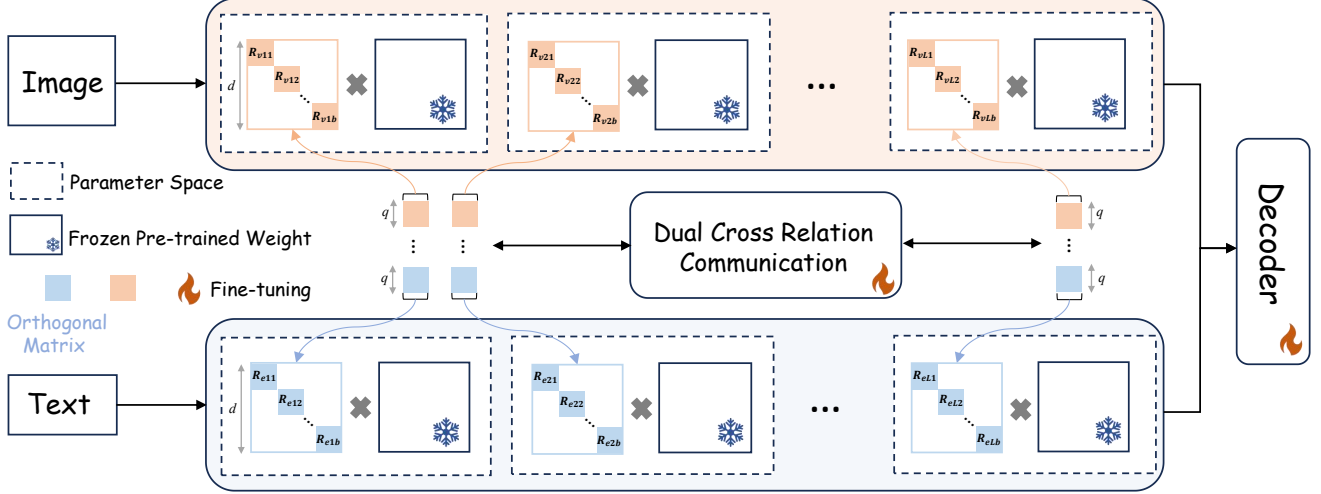


Figure 1. **A schematic representation of H-CLIP.** In the H-CLIP framework, we propose a partial orthogonal fine-tuning strategy, where each pre-trained weight matrix is paired with a tuned block-diagonal transformation matrix, some of which are orthogonal to preserve generalization. Then, we introduce a dual cross-relation communication mechanism to facilitate communication among all matrices, enabling alignment between different modalities.

using a small number of parameters. However, this approach can cause a misalignment between image and text features in CLIP, resulting in sub-optimal performance [56]. Based on the above analysis, we introduce Dual Cross-Relation Communication (DCRC), which facilitates interaction among different layers and modalities (i.e., text and image). DCRC explicitly enhances the flexibility of fine-tuned projection adjustments and prevents misalignment issues.

DCRC introduces cross-layer and cross-modality communication among different block-diagonal matrices, achieved through two relation projections. To do this, we first treat all blocks in ℓ^{th} layer as an individual slice in this 3-order tensor \mathcal{T}_ℓ , which is derived as follows:

$$\mathcal{T}_\ell = [\mathbf{R}_{v\ell 1}, \mathbf{R}_{v\ell 1}, \dots, \mathbf{R}_{v\ell i}, \mathbf{R}_{v\ell i}, \dots, \mathbf{R}_{v\ell b}, \mathbf{R}_{v\ell b}] \in \mathbb{R}^{q \times q \times (b+b)}, \quad (8)$$

where $q = d/b$. Then, we treat the tensor \mathcal{T}_ℓ as an individual slice within a 4-order tensor \mathcal{T} , defined as follows:

$$\mathcal{T} = [\mathcal{T}_1, \mathcal{T}_2, \dots, \mathcal{T}_\ell, \dots, \mathcal{T}_L] \in \mathbb{R}^{q \times q \times (b+b) \times L}. \quad (9)$$

Initially, according to the characteristics of gradient propagation in deep learning theory, i.e., chain rule, each frontal slice $\mathbf{R}_{v\ell i} \in \{\mathbb{R}^{q \times q}\}^{(b+b) \times L}$ is updated sequentially in CLIP's encoder. As a result, updating the \mathcal{T} lacks cross-frontal-slice communication, limiting the flexibility of adjusting fine-tuned projection. To address this, we introduce two special tensor products, i.e., **3-order T-product** and **Higher-order T-product**.

Definition 4.1(3-order T-product) For $\mathcal{A} \in \mathbb{R}^{n_1 \times n_2 \times n_3}$ and $\mathcal{B} \in \mathbb{R}^{n_2 \times l \times n_3}$, the 3-order T-product $\mathcal{C} \in \mathbb{R}^{n_1 \times l \times n_3} = \mathcal{A} * \mathcal{B}$ is defined as:

$$\mathbb{R}^{n_1 \times l \times n_3} = \mathcal{A} * \mathcal{B} \text{ is defined as:}$$

$$\mathcal{C} = \mathcal{A} * \mathcal{B} = \text{fold}(\text{circ}(\mathcal{A}) \cdot \text{unfold}(\mathcal{B})), \quad (10)$$

where “*” represents a tensor product, “.” represents standard matrix product.

Definition 4.2(Higher-order T-product) For $\mathcal{A} \in \mathbb{R}^{n_1 \times n_2 \times n_3 \times \dots \times n_p}$ and $\mathcal{B} \in \mathbb{R}^{n_2 \times l \times n_3 \times \dots \times n_p}$, the Higher-order T-product $\mathcal{C} \in \mathbb{R}^{n_1 \times l \times n_3 \times \dots \times n_p} = \mathcal{A} * \mathcal{B}$ is defined as:

$$\mathcal{C} = \mathcal{A} * \mathcal{B} = \text{fold}(\text{circ}(\mathcal{A}) * \text{unfold}(\mathcal{B})). \quad (11)$$

If $\mathcal{A} \in \mathbb{R}^{n_1 \times n_2 \times n_3}$, according to the **3-order T-product**, there is an invertible transform $S_3(\cdot) : \mathbb{R}^{n_1 \times n_2 \times n_3} \rightarrow \mathbb{R}^{n_1 \times n_2 \times n_3}$ in third dimension and it transform the Eq. (10) as:

$$\begin{aligned} \mathcal{C} &= S_3^{-1}(S_3(\mathcal{A}) \odot S_3(\mathcal{B})) \\ &= S_3^{-1}(\bar{\mathcal{A}} \odot \bar{\mathcal{B}}) = S_3^{-1}(\bar{\mathcal{C}}), \end{aligned} \quad (12)$$

where $\bar{\mathcal{C}} = \bar{\mathcal{A}} \odot \bar{\mathcal{B}}$ denotes the frontal-slice-wise product (Definition 2.1 refers to [21]) $\bar{\mathcal{C}}(\cdot, \cdot, i) = \bar{\mathcal{A}}(\cdot, \cdot, i) \cdot \bar{\mathcal{B}}(\cdot, \cdot, i)$, $i = 1, 2, \dots, n_3$ and $S_3^{-1}(\cdot)$ is the inverse transform of $S_3(\cdot)$. According to the definition of the frontal-slice-wise product, the invertible transform $S_3(\cdot)$ is formulated as:

$$\bar{\mathcal{A}} = S_3(\mathcal{A}) = \mathcal{A} \times_3 \mathbf{S}_3, \quad (13)$$

where “ \times_3 ” denotes the mode-3 product and $\mathbf{S}_3 \in \mathbb{R}^{n_3 \times n_3}$ is an arbitrary invertible matrix. Similarly, the inverse transform of Eq. (13) is derived as:

$$\mathcal{A} = S_3^{-1}(\bar{\mathcal{A}}) = \bar{\mathcal{A}} \times_3 \mathbf{S}_3^{-1}. \quad (14)$$

Similarly, if $\mathcal{A} \in \mathbb{R}^{n_1 \times n_2 \times \dots \times n_p}$, according to the **Higer-order T-product**, there are invertible transform $S_i(\cdot) : \mathbb{R}^{n_1 \times n_2 \times \dots \times n_p} \rightarrow \mathbb{R}^{n_1 \times n_2 \times \dots \times n_p}, i = 3, 4, \dots, p$ in i^{th} dimension and they transform the Eq. (11) as:

$$\mathcal{C} = \tilde{S}^{-1}(\tilde{S}(\mathcal{A}) \odot \tilde{S}(\mathcal{B})) = \tilde{S}^{-1}(\bar{\mathcal{A}} \odot \bar{\mathcal{B}}) = \tilde{S}^{-1}(\bar{\mathcal{C}}), \quad (15)$$

where $\tilde{S}(\mathcal{A}) = S_p(S_{p-1}(\dots S_3(\mathcal{A}) \dots)), \bar{\mathcal{C}} = \bar{\mathcal{A}} \odot \bar{\mathcal{B}}$ denotes the frontal-slice-wise product $\bar{\mathcal{C}}(\cdot, \cdot, \cdot, i) = \bar{\mathcal{A}}(\cdot, \cdot, \cdot, i) \cdot \bar{\mathcal{B}}(\cdot, \cdot, \cdot, i), i = 1, 2, \dots, n_3 n_4 \dots n_p$ and $\tilde{S}^{-1}(\cdot)$ is the inverse transform of $\tilde{S}(\cdot)$. Similarly, the inverse transform $\tilde{S}(\cdot)$ is formulated as:

$$\bar{\mathcal{A}} = \tilde{S}(\mathcal{A}) = \mathcal{A} \times_3 \mathbf{S}_3 \times_4 \mathbf{S}_4 \dots \times_p \mathbf{S}_p, \quad (16)$$

and its inverse transform is derived as:

$$\mathcal{A} = \tilde{S}^{-1}(\bar{\mathcal{A}}) = \bar{\mathcal{A}} \times_3 \mathbf{S}_3^{-1} \times_4 \mathbf{S}_4^{-1} \dots \times_p \mathbf{S}_p^{-1}. \quad (17)$$

Derivation. please refer to supplementary material. ■

According to Eqs. (15), (16) and (17), we adopt its idea and design arbitrary invertible relation matrix $\mathbf{S}_3 \in \mathbb{R}^{(b+b) \times (b+b)}$ and $\mathbf{S}_4 \in \mathbb{R}^{L \times L}$ to capture the cross-modality and cross-layer information in \mathcal{T} . Then the updated tensor \mathcal{T}_w is formulated as:

$$\mathcal{T}_w = \mathcal{T} \times_3 \mathbf{S}_3 \times_4 \mathbf{S}_4 \in \mathbb{R}^{q \times q \times (b+b) \times L}, \quad (18)$$

where the relation matrix \mathbf{S}_3 and \mathbf{S}_4 are learnable. To better capture the nonlinear interactions inside the whole parameter space, we further adopt k layers deep neural network (DNN) $f_3(\cdot)$ and $f_4(\cdot)$ to replace the transform $\times_3 \mathbf{S}_3$ and $\times_4 \mathbf{S}_4$, respectively, and the DNN $f_3(\cdot)$ is formulated as:

$$f_3(\mathcal{T}) = \sigma(\dots \sigma(\mathcal{A} \times_3 \mathbf{W}_1) \dots) \times_3 \mathbf{W}_k, \quad (19)$$

where $\sigma(\cdot)$ is a nonlinear scalar function and matrices $\{\mathbf{W}_j \in \mathbb{R}^{(b+b)}\}_{j=1}^k$. The DNN $f_4(\cdot)$ is similar. Finally, the \mathcal{T} is updated by $\mathcal{T} = \mathcal{T} + \alpha \mathcal{T}_w$, where $\alpha \in \mathbb{R}^{(b+b) \times L}$ is a learnable parameter.

4.4. Overall Architecture

Overall, we develop a H-CLIP framework, and for an input feature map \mathbf{M}_ℓ in the ℓ^{th} Transformer layer of CLIP, the adjusted feature map provided by H-CLIP, $\tilde{\mathbf{M}}_\ell$, is formally via:

$$\tilde{\mathbf{M}}_\ell = \mathcal{F}_\ell(\mathbf{M}_\ell; \mathcal{T}_\ell \mathbf{W}_\ell). \quad (20)$$

where \mathbf{W}_ℓ is a pre-trained weight matrix in ℓ^{th} layer of CLIP's encoder, \mathcal{T}_ℓ is a 3-order tensor that is comprised of all the matrices \mathbf{R} in ℓ^{th} layer, and \mathcal{F}_ℓ represents ℓ^{th} layer of CLIP's encoder.

Fine-tuning Stage. During the fine-tuning phase, H-CLIP is fine-tuned in conjunction with the original parameter space of CLIP, which is loaded from the pre-trained checkpoint and remains frozen.

Loss Function. Following previous works [7, 52], we incorporate a cross-entropy loss, denoted as \mathcal{L}_{ce} , for the fine-tuning of CLIP.

5. Experiments

5.1. Experimental Setup

Datasets. Following previous studies [7, 52], we utilize the COCO-Stuff dataset [2] as our training set. This dataset comprises approximately 118,000 densely annotated images across 171 distinct semantic categories. During inference, we carry out comparisons with state-of-the-art methods across several semantic segmentation datasets, including ADE20K [59], PASCAL VOC [12], and PASCAL-Context [37].

- **ADE20K** [59] is a classical semantic segmentation dataset comprising around 20,000 training images and 2,000 validation images. Besides, it includes two different test sets: A-150 and A-847. The test set A-150 has 150 common categories, while the test set A-847 has 847 categories.
- **PASCAL VOC** [12] is a small dataset for semantic segmentation, which includes 1464 training images and 1449 validation images. The dataset contains 20 different foreground categories. We name it as PAS-20. In line with [7], we also report a score on PAS-20^b, which involves “background” as the 21st category.
- **PASCAL-Context** [37] is upgraded from the original PASCAL VOC dataset. It includes two different test sets: PC-59 and PC-459 for evaluation. The test set PC-59 has 59 categories, while the test set PC-459 has 459 categories.

Evaluation metric. Following prior works [7, 52], we adopt mean Intersection over Union (mIoU) to evaluate the semantic segmentation performance on the three benchmarks.

Implementation Details. We implement our method using the Transformer-based CLIP model. Following the protocol established in [7], we evaluate our results on two versions of the CLIP model: ViT-B/16 and ViT-L/14. For training, we use the Adam optimizer [23] with an initial learning rate of 5×10^{-6} for CLIP, and a weight decay of 10^{-4} . Training is conducted with one image per mini-batch. We set $q = 128$ for balancing efficiency and performance. The function $f_3(\cdot)$ and $f_4(\cdot)$ are implemented using two 2-layer MLPs. We act the cost-based approach provided in [7] as our decoder. All models are trained over 80,000 iterations on 4 NVIDIA RTX 3090 GPUs.

5.2. Main Results

Comparing to SOTAs. Here, we compare our proposed H-CLIP with several state-of-the-art methods, as shown in Table 1, using six test sets across three benchmarks. Overall, we achieve the best results. Most existing open-vocabulary semantic segmentation methods employ traditional fine-tuning approaches, i.e., full or partial fine-tuning (tuning certain layers of CLIP). While these methods offer sufficient flexibility for learning new knowledge, they often result in a significant performance drop on unseen classes,

Model	VLM	Additional Backbone	Fine-tuning Space	A-847	PC-459	A-150	PC-59	PAS-20	PAS-20 ^b
Traditional Fine-Tuning									
ZS3Net [1]	-	ResNet-101	E	-	-	-	19.4	38.3	-
LSeg [26]	CLIP ViT-B/32	ResNet-101	E	-	-	-	-	47.4	-
ZegFormer [8]	CLIP ViT-B/16	ResNet-101	E	4.9	9.1	16.9	42.8	86.2	62.7
ZSseg [54]	CLIP ViT-B/16	ResNet-101	E	7.0	-	20.5	47.7	88.4	-
OpenSeg [15]	ALIGN	ResNet-101	E	4.4	7.9	17.5	40.1	-	63.8
OVSeg [32]	CLIP ViT-B/16	ResNet-101c	E	7.1	11.0	24.8	53.3	92.6	-
ZegCLIP [63]	CLIP ViT-B/16	-	E	-	-	-	41.2	93.6	-
SED [52]	CLIP ConvNeXt-B	-	E	11.4	18.6	31.6	57.3	94.4	-
CAT-Seg [7]	CLIP ViT-B/16	-	E	<u>12.0</u>	<u>19.0</u>	<u>31.8</u>	<u>57.5</u>	<u>94.6</u>	<u>77.3</u>
Parameter-efficient Fine-Tuning									
SAN [55]	CLIP ViT-B/16	Side Adapter	E	10.1	12.6	27.5	53.8	94.0	-
Ours	CLIP ViT-B/16	-	H	12.5	19.4	32.4	57.9	95.2	78.2
Traditional Fine-Tuning									
LSeg [26]	CLIP ViT-B/32	ViT-L/16	E	-	-	-	-	52.3	-
OpenSeg [15]	ALIGN	Eff-B7	E	8.1	11.5	26.4	44.8	-	70.2
OVSeg [32]	CLIP ViT-L/14	Swin-B	E	9.0	12.4	29.6	55.7	94.5	-
SAN [55]	CLIP ViT-L/14	-	E	12.4	15.7	32.1	57.7	94.6	-
ODISE [53]	CLIP ViT-L/14	Stable Diffusion	E	11.1	14.5	29.9	57.3	-	-
SED [52]	CLIP ConvNeXt-L	-	E	13.9	22.6	35.2	60.6	96.1	-
FC-CLIP [56]	CLIP ConvNeXt-L	-	E	14.8	18.2	34.1	58.4	95.4	-
CAT-Seg [7]	CLIP ViT-L/14	-	E	<u>16.0</u>	<u>23.8</u>	<u>37.9</u>	<u>63.3</u>	<u>97.0</u>	<u>82.5</u>
Parameter-efficient Fine-Tuning									
SAN [55]	CLIP ViT-L/14	Side Adapter	E	12.4	15.7	32.1	57.7	94.6	-
Ours	CLIP ViT-L/14	-	H	16.5	24.2	38.4	64.1	97.7	83.2

Table 1. **Comparison with state-of-the-art methods on standard benchmarks.** The best-performing results are presented in bold, while the second-best results are underlined. “E”: Euclidean Space. “H”: Hypersphere Space.

Methods	OVSeg [32]	CAT-Seg [7]	SAN [55]	Ours
Param. (M)	147.2	25.6	8.4	5.6

Table 2. **Efficiency comparison** in terms of learnable parameters.

as observed with OVSeg [32]. Among these methods, CAT-Seg [7] achieves performance comparable to ours. However, its fine-tuning scheme is manually controlled through different layer combinations, necessitating a careful design to balance generalization and flexibility, while ours does not suffer from such an issue. Then, compared to SAN [55], another parameter-efficient fine-tuning method that introduces only a limited number of tunable parameters, our approach significantly outperforms it, achieving improvements of 6.6% on the PC-459 dataset and 3.9% on the PC-59 dataset with ViT-B/16 as the base model. These results demonstrate the effectiveness of our method in preserving generalization while learning segmentation knowledge.

Qualitative results. Here, we visualize our method’s representative example segmentation results against prevailing methods, e.g., CAT-Seg [7] in the A-150 dataset. As shown

in Figs. 2, we observe that our approach is able to generalize on diverse scenarios and produce more accurate results. More visualizations can be found in supplemental materials.

Efficiency comparison. We compare the efficiency of our method with other approaches, including OVSeg [32], CAT-Seg [7], and SAN [55], all of which utilize CLIP ViT models. The comparison, summarized in Table 2, shows that our method employs the fewest trainable parameters while balancing the generalization of the pre-trained model and the flexibility for learning new knowledge. Additionally, since we introduce a lightweight architecture for calculating relations, specifically two relation matrices, the inference overhead is negligible during the inference phase.

Generalization on other dense prediction tasks. We validate our method on an open-vocabulary object detection task and experiment on COCO dataset following [51] in Table 5. The results demonstrate that our method can generalize to mainstream dense prediction tasks, including segmentation and detection.

5.3. Ablative Studies

Ablation of Main Components. Here, we conduct an ablation study to demonstrate the benefits of each component of

Method	POP	DCRC	Parameter counts (M)	A-847	PC-459	A-150	PC-59	PAS-20	PAS-20 ^b
Freeze	-	-	0	4.4	6.6	24.8	49.4	92.5	71.9
Methods for Parameter-efficient Fine-Tuning									
LoRA [17]	-	-	7.5	11.4	17.6	28.6	55.1	94.2	76.7
OFT [40]	-	-	3.8	10.9	18.0	30.2	53.7	93.7	74.3
VPT [19]	-	-	2.2	5.7	10.2	23.7	54.3	93.8	75.1
Adapter [16]	-	-	7.5	10.4	16.5	28.8	54.9	94.2	75.2
LST [45]	-	-	19.8	7.2	12.7	27.0	56.8	95.4	76.3
SSF [31]	-	-	0.6	6.9	15.2	28.6	52.1	93.2	72.8
Ours									
H-CLIP	✓	✗	5.62	12.3	19.0	31.6	56.4	94.6	76.3
	✗	✓	0.01	7.6	10.9	26.8	53.6	92.7	74.5
	✓	✓	5.63	12.5	19.4	32.4	57.9	95.2	78.2

Table 3. **Ablation study on the components of H-CLIP** and universal PEFT methods, i.e., “LoRA” [17], “OFT” [40], “VPT” [19], “Adapter” [16], “LST” [45] and “SSF” [31]. “POP”: Partial Orthogonal Parameterization. “DCRC”: Dual Cross Relation Communication. Towards easy to compare, we exclude the segmentation decoder when calculating the number of learnable parameters. The base model is ViT-B/16.

	Block dimension q	Parameter counts (M)	A-847	PC-459	A-150	PC-59	PAS-20	PAS-20 ^b
(a)	256 × 256	22.52	12.4	19.2	32.7	57.6	95.4	77.9
	128 × 128	5.63	12.5	19.4	32.4	57.9	95.2	78.2
	64 × 64	1.41	11.7	18.4	31.7	56.9	95.0	76.4
Orthogonal Constraint								
(b)	w/o	7.51	11.9	18.5	32.2	57.5	95.3	76.9
	with	3.76	12.2	19.1	31.4	57.1	94.3	76.8
	POP	5.63	12.5	19.4	32.4	57.9	95.2	78.2

Table 4. **Ablation study on different designs in POP**. We show the impact of (a) different block dimensions q and (b) orthogonal constraints. The base model is ViT-B/16.

Methods	$\mathbf{AP}_{50}^{\text{Base}}$	$\mathbf{AP}_{50}^{\text{Novel}}$
CLIP	21.6	36.4
Traditional Fine-Tuning		
CLIM [51]	25.7	42.5
Parameter-efficient Fine-Tuning		
LoRA [17]	24.4	41.5
H-CLIP	25.1	42.9

Table 5. **Comparisons on fine-tuning CLIP for an open-vocabulary object detection task** on the COCO dataset [33]. Results are measured by the box AP at IoU threshold 0.5.

our proposed H-CLIP: partial orthogonal fine-tuning (POP) and dual cross-relation communication (DCRC). We use the ViT-B/16 [9] version of CLIP as the baseline, shown in row 1 of Table 3. Additionally, we implement a mainstream parameter-efficient fine-tuning (PEFT) method, LoRA [17],

for comparison with a similar number of learnable parameters, as shown in row 2. Note that LoRA can improve performance compared to the baseline, demonstrating that PEFT is a viable approach for this task. However, the goal of traditional PEFT methods, which update weights using a small number of learnable parameters, does not necessarily preserve the generalization capability of pre-trained CLIP. In contrast, we introduce the principle of hyperspherical energy, which effectively ensures the minimum undermining of CLIP’s intrinsic semantic structure, resulting in improved performance. Then, comparing row 5 to row 2, we observe significant performance gains, indicating that our results are driven by our targeted solution rather than merely the number of parameters. Moreover, row 3 shows that using only POP preserves generalization on unseen classes, particularly in the A-847 dataset. Meanwhile, solely adapting DCRC shows limited improvement, as it only enhances communication among frozen weight matrices. Finally, integrating DCRC with POP yields clear performance gains, e.g., a

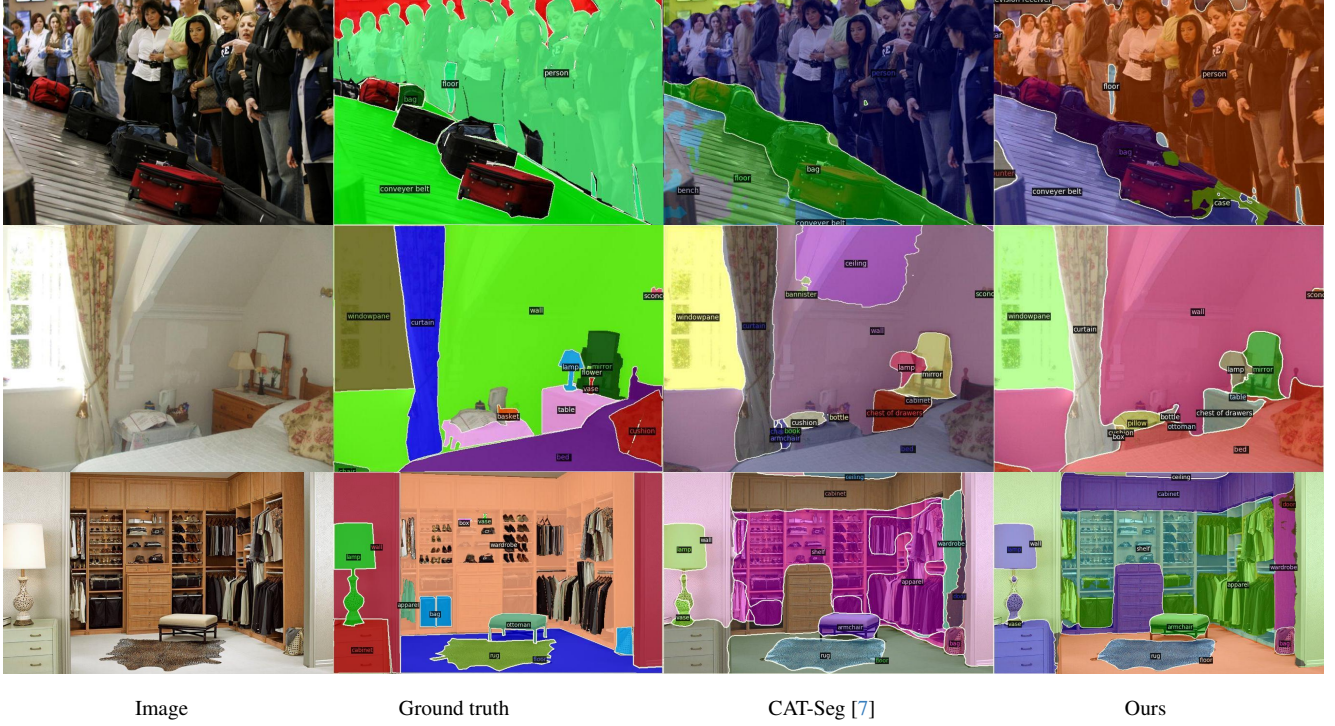


Figure 2. Comparison of qualitative results on ADE20K [59] with 150 categories. We compare H-CLIP with a state-of-the-art method, i.e., CAT-Seg [7].

12.6% improvement on the PC-459 dataset.

Discussion of POP. Table 4 presents experiments introducing different designs into POP. The design of POP is related to (1) block dimension, i.e., q , and (2) how orthogonality constraints are applied. In (a), the results show that larger q generally performs better than smaller q . However, we find a good trade-off between performance and parameter efficiency, with $q = 128$ working well across datasets and tasks. Therefore, we maintain this setting in other experiments. In (b), we show that both blindly applying orthogonality constraints to the learnable matrices of all layers and not using any constraints at all can degrade performance on several datasets, demonstrating the value of our analysis with the hyperspherical energy principle. Notably, when we adopt orthogonal constraints on both CLIP’s image and text encoders to strictly maintain the original semantic structures, it is similar to equipping OFT [40] with our proposed DCRC module. Differently, our method applies orthogonal constraints only to the text encoder. This is crucial for open-vocabulary semantic segmentation, as it can provide more flexibility in fine-tuning the image encoder, facilitating the transfer of CLIP’s initial alignment from image-level to pixel-level.

6. Conclusion

In this paper, we propose a H-CLIP framework to address three issues: 1) high computational cost, 2) misalignment between the two inherent modalities of CLIP, and 3) degraded generalization ability on unseen categories when equipping CLIP with pixel-level prediction ability for open-vocabulary semantic segmentation. Specifically, we propose a symmetrical parameter-efficient fine-tuning (PEFT) strategy conducted in hyperspherical space for both of the two CLIP modalities. Specifically, the PEFT strategy is achieved by a series of efficient block-diagonal learnable transformation matrices and a dual cross-relation communication module among all learnable matrices to mitigate misalignment between different modalities. Furthermore, we apply an additional constraint to PEFT on the CLIP text encoder according to the hyperspherical energy principle, i.e., minimizing hyperspherical energy during fine-tuning preserves the intrinsic structure of the original parameter space, to prevent the destruction of the generalization ability offered by the CLIP text encoder. Extensive experiments demonstrate that the proposed H-CLIP framework generalized improves segmentation performance across several benchmarks while introducing approximately 4% of CLIP’s total parameters. We hope our approach will provide a new direction and inspire future research in this field.

References

[1] Maxime Bucher, Tuan-Hung Vu, Matthieu Cord, and Patrick Pérez. Zero-shot semantic segmentation. *Advances in Neural Information Processing Systems*, 32, 2019. 6

[2] Holger Caesar, Jasper Uijlings, and Vittorio Ferrari. Coco-stuff: Thing and stuff classes in context. In *Proceedings of the IEEE conference on computer vision and pattern recognition*, pages 1209–1218, 2018. 1, 2, 5

[3] Arthur Cayley. Sur quelques propriétés des déterminants gauches. 1846. 3

[4] Tianrun Chen, Lanyun Zhu, Chaotao Ding, Runlong Cao, Shangzhan Zhang, Yan Wang, Zejian Li, Lingyun Sun, Papa Mao, and Ying Zang. Sam fails to segment anything? – sam-adapter: Adapting sam in underperformed scenes: Camouflage, shadow, and more, 2023. 2

[5] Yen-Chun Chen, Linjie Li, Licheng Yu, Ahmed El Kholy, Faisal Ahmed, Zhe Gan, Yu Cheng, and Jingjing Liu. Uniter: Universal image-text representation learning. In *European conference on computer vision*, pages 104–120. Springer, 2020. 1

[6] Bowen Cheng, Ishan Misra, Alexander G Schwing, Alexander Kirillov, and Rohit Girdhar. Masked-attention mask transformer for universal image segmentation. In *Proceedings of the IEEE/CVF conference on computer vision and pattern recognition*, pages 1290–1299, 2022. 2

[7] Seokju Cho, Heeseong Shin, Sunghwan Hong, Anurag Arnab, Paul Hongsuck Seo, and Seungryong Kim. Cat-seg: Cost aggregation for open-vocabulary semantic segmentation, 2024. 1, 2, 5, 6, 8

[8] Jian Ding, Nan Xue, Gui-Song Xia, and Dengxin Dai. Decoupling zero-shot semantic segmentation. In *Proceedings of the IEEE/CVF Conference on Computer Vision and Pattern Recognition*, pages 11583–11592, 2022. 2, 6

[9] Alexey Dosovitskiy, Lucas Beyer, Alexander Kolesnikov, Dirk Weissenborn, Xiaohua Zhai, Thomas Unterthiner, Mostafa Dehghani, Matthias Minderer, Georg Heigold, Sylvain Gelly, et al. An image is worth 16x16 words: Transformers for image recognition at scale. *arXiv preprint arXiv:2010.11929*, 2020. 7

[10] Zi-Yi Dou, Aishwarya Kamath, Zhe Gan, Pengchuan Zhang, Jianfeng Wang, Linjie Li, Zicheng Liu, Ce Liu, Yann Le-Cun, Nanyun Peng, et al. Coarse-to-fine vision-language pre-training with fusion in the backbone. *Advances in neural information processing systems*, 35:32942–32956, 2022. 1

[11] Zi-Yi Dou, Yichong Xu, Zhe Gan, Jianfeng Wang, Shuohang Wang, Lijuan Wang, Chenguang Zhu, Pengchuan Zhang, Lu Yuan, Nanyun Peng, et al. An empirical study of training end-to-end vision-and-language transformers. In *Proceedings of the IEEE/CVF Conference on Computer Vision and Pattern Recognition*, pages 18166–18176, 2022. 1

[12] Mark Everingham, Luc Van Gool, Christopher KI Williams, John Winn, and Andrew Zisserman. The pascal visual object classes (voc) challenge. *International journal of computer vision*, 88:303–338, 2010. 5

[13] Zhe Gan, Yen-Chun Chen, Linjie Li, Chen Zhu, Yu Cheng, and Jingjing Liu. Large-scale adversarial training for vision-and-language representation learning. *Advances in Neural Information Processing Systems*, 33:6616–6628, 2020. 1

[14] Peng Gao, Shijie Geng, Renrui Zhang, Teli Ma, Rongyao Fang, Yongfeng Zhang, Hongsheng Li, and Yu Qiao. Clip-adapter: Better vision-language models with feature adapters. *International Journal of Computer Vision*, 132(2):581–595, 2024. 2

[15] Golnaz Ghiasi, Xiuye Gu, Yin Cui, and Tsung-Yi Lin. Scaling open-vocabulary image segmentation with image-level labels. In *European Conference on Computer Vision*, pages 540–557. Springer, 2022. 2, 6

[16] Neil Houlsby, Andrei Giurgiu, Stanislaw Jastrzebski, Bruna Morrone, Quentin De Laroussilhe, Andrea Gesmundo, Mona Attariyan, and Sylvain Gelly. Parameter-efficient transfer learning for nlp. In *International conference on machine learning*, pages 2790–2799. PMLR, 2019. 7

[17] Edward J Hu, Yelong Shen, Phillip Wallis, Zeyuan Allen-Zhu, Yuanzhi Li, Shean Wang, Lu Wang, and Weizhu Chen. LoRA: Low-rank adaptation of large language models. In *International Conference on Learning Representations*, 2022. 7

[18] Zhicheng Huang, Zhaoyang Zeng, Yupan Huang, Bei Liu, Dongmei Fu, and Jianlong Fu. Seeing out of the box: End-to-end pre-training for vision-language representation learning. In *Proceedings of the IEEE/CVF Conference on Computer Vision and Pattern Recognition*, pages 12976–12985, 2021. 1

[19] Menglin Jia, Luming Tang, Bor-Chun Chen, Claire Cardie, Serge Belongie, Bharath Hariharan, and Ser-Nam Lim. Visual prompt tuning. In *European Conference on Computer Vision*, pages 709–727. Springer, 2022. 7

[20] Aishwarya Kamath, Mannat Singh, Yann LeCun, Gabriel Synnaeve, Ishan Misra, and Nicolas Carion. Mdetr-modulated detection for end-to-end multi-modal understanding. In *Proceedings of the IEEE/CVF International Conference on Computer Vision*, pages 1780–1790, 2021. 1

[21] Eric Kernfeld, Misha Kilmer, and Shuchin Aeron. Tensor–tensor products with invertible linear transforms. *Linear Algebra and its Applications*, 485:545–570, 2015. 4

[22] Wonjae Kim, Bokyung Son, and Ildoo Kim. Vilt: Vision-and-language transformer without convolution or region supervision. In *International conference on machine learning*, pages 5583–5594. PMLR, 2021. 1

[23] Diederik P Kingma and Jimmy Ba. Adam: A method for stochastic optimization. *arXiv preprint arXiv:1412.6980*, 2014. 5

[24] Alexander Kirillov, Eric Mintun, Nikhila Ravi, Hanzi Mao, Chloe Rolland, Laura Gustafson, Tete Xiao, Spencer Whitehead, Alexander C Berg, Wan-Yen Lo, et al. Segment anything. In *Proceedings of the IEEE/CVF International Conference on Computer Vision*, pages 4015–4026, 2023. 2

[25] Jungbeom Lee, Jooyoung Choi, Jisoo Mok, and Sungroh Yoon. Reducing information bottleneck for weakly supervised semantic segmentation. *Advances in Neural Information Processing Systems*, 34:27408–27421, 2021. 3

[26] Boyi Li, Kilian Q Weinberger, Serge Belongie, Vladlen Koltun, and Rene Ranftl. Language-driven semantic segmentation. In *International Conference on Learning Representations*, 2022. 1, 3, 6

[27] Junnan Li, Ramprasaath Selvaraju, Akhilesh Gotmare, Shafiq Joty, Caiming Xiong, and Steven Chu Hong Hoi. Align before fuse: Vision and language representation learning with momentum distillation. *Advances in neural information processing systems*, 34:9694–9705, 2021. 1

[28] Junnan Li, Dongxu Li, Caiming Xiong, and Steven Hoi. Blip: Bootstrapping language-image pre-training for unified vision-language understanding and generation. In *International conference on machine learning*, pages 12888–12900. PMLR, 2022. 2

[29] Liunian Harold Li, Pengchuan Zhang, Haotian Zhang, Jianwei Yang, Chunyuan Li, Yiwu Zhong, Lijuan Wang, Lu Yuan, Lei Zhang, Jenq-Neng Hwang, et al. Grounded language-image pre-training. In *Proceedings of the IEEE/CVF Conference on Computer Vision and Pattern Recognition*, pages 10965–10975, 2022. 2

[30] Xiuju Li, Xi Yin, Chunyuan Li, Pengchuan Zhang, Xiaowei Hu, Lei Zhang, Lijuan Wang, Houdong Hu, Li Dong, Furu Wei, et al. Oscar: Object-semantics aligned pre-training for vision-language tasks. In *Computer Vision–ECCV 2020: 16th European Conference, Glasgow, UK, August 23–28, 2020, Proceedings, Part XXX 16*, pages 121–137. Springer, 2020. 1

[31] Dongze Lian, Daquan Zhou, Jia Shi Feng, and Xinchao Wang. Scaling & shifting your features: A new baseline for efficient model tuning. *Advances in Neural Information Processing Systems*, 35:109–123, 2022. 7

[32] Feng Liang, Bichen Wu, Xiaoliang Dai, Kunpeng Li, Yinan Zhao, Hang Zhang, Peizhao Zhang, Peter Vajda, and Diana Marculescu. Open-vocabulary semantic segmentation with mask-adapted clip. In *Proceedings of the IEEE/CVF Conference on Computer Vision and Pattern Recognition*, pages 7061–7070, 2023. 2, 3, 6

[33] Tsung-Yi Lin, Michael Maire, Serge Belongie, James Hays, Pietro Perona, Deva Ramanan, Piotr Dollár, and C Lawrence Zitnick. Microsoft coco: Common objects in context. In *Computer Vision–ECCV 2014: 13th European Conference, Zurich, Switzerland, September 6–12, 2014, Proceedings, Part V 13*, pages 740–755. Springer, 2014. 7

[34] Haotian Liu, Chunyuan Li, Qingyang Wu, and Yong Jae Lee. Visual instruction tuning. *Advances in neural information processing systems*, 36, 2024. 2

[35] Weiyang Liu, Rongmei Lin, Zhen Liu, Lixin Liu, Zhiding Yu, Bo Dai, and Le Song. Learning towards minimum hyperspherical energy. *Advances in neural information processing systems*, 31, 2018. 1

[36] Jiasen Lu, Dhruv Batra, Devi Parikh, and Stefan Lee. Vilbert: Pretraining task-agnostic visiolinguistic representations for vision-and-language tasks. *Advances in neural information processing systems*, 32, 2019. 1, 2

[37] Roozbeh Mottaghi, Xianjie Chen, Xiaobai Liu, Nam-Gyu Cho, Seong-Whan Lee, Sanja Fidler, Raquel Urtasun, and Alan Yuille. The role of context for object detection and semantic segmentation in the wild. In *Proceedings of the IEEE conference on computer vision and pattern recognition*, pages 891–898, 2014. 5

[38] Zelin Peng, Zhengqin Xu, Zhilin Zeng, Lingxi Xie, Qi Tian, and Wei Shen. Parameter efficient fine-tuning via cross block orchestration for segment anything model. In *IEEE/CVF Conference on Computer Vision and Pattern Recognition (CVPR)*, 2024. 2, 3

[39] Zelin Peng, Zhengqin Xu, Zhilin Zeng, Xiaokang Yang, and Wei Shen. Sam-parser: Fine-tuning sam efficiently by parameter space reconstruction. In *Proceedings of the AAAI Conference on Artificial Intelligence*, pages 4515–4523, 2024. 2

[40] Zeju Qiu, Weiyang Liu, Haiwen Feng, Yuxuan Xue, Yao Feng, Zhen Liu, Dan Zhang, Adrian Weller, and Bernhard Schölkopf. Controlling text-to-image diffusion by orthogonal finetuning. *Advances in Neural Information Processing Systems*, 36:79320–79362, 2023. 1, 3, 7, 8

[41] Alec Radford, Jong Wook Kim, Chris Hallacy, Aditya Ramesh, Gabriel Goh, Sandhini Agarwal, Girish Sastry, Amanda Askell, Pamela Mishkin, Jack Clark, et al. Learning transferable visual models from natural language supervision. In *International conference on machine learning*, pages 8748–8763. PMLR, 2021. 1, 2

[42] Baptiste Roziere, Jonas Gehring, Fabian Gloclekle, Sten Sootla, Itai Gat, Xiaoqing Ellen Tan, Yossi Adi, Jingyu Liu, Tal Remez, Jérémie Rapin, et al. Code llama: Open foundation models for code. *arXiv preprint arXiv:2308.12950*, 2023. 2

[43] Amanpreet Singh, Ronghang Hu, Vedanuj Goswami, Guillaume Couairon, Wojciech Galuba, Marcus Rohrbach, and Douwe Kiela. Flava: A foundational language and vision alignment model. In *Proceedings of the IEEE/CVF Conference on Computer Vision and Pattern Recognition*, pages 15638–15650, 2022.

[44] Weijie Su, Xizhou Zhu, Yue Cao, Bin Li, Lewei Lu, Furu Wei, and Jifeng Dai. Vi-bert: Pre-training of generic visual-linguistic representations. *arXiv preprint arXiv:1908.08530*, 2019. 2

[45] Yi-Lin Sung, Jaemin Cho, and Mohit Bansal. Lst: Ladder side-tuning for parameter and memory efficient transfer learning. *Advances in Neural Information Processing Systems*, 35: 12991–13005, 2022. 7

[46] Hao Tan and Mohit Bansal. Lxmert: Learning cross-modality encoder representations from transformers. *arXiv preprint arXiv:1908.07490*, 2019. 1

[47] JJ Tomson. On the structure of the atom: an investigation of the stability and periods of oscillation of a number of corpuscles arranged at equal intervals around the circumference of a circle; with application of the results to the theory atomic structure. *Philos. Mag. Series 6*, 7(39):237, 1904. 2

[48] Jianfeng Wang, Xiaowei Hu, Zhe Gan, Zhengyuan Yang, Xiyang Dai, Zicheng Liu, Yumao Lu, and Lijuan Wang. Ufo: A unified transformer for vision-language representation learning. *arXiv preprint arXiv:2111.10023*, 2021. 1

[49] Zifeng Wang, Xi Chen, Rui Wen, Shao-Lun Huang, Ercan Kuruoglu, and Yefeng Zheng. Information theoretic counterfactual learning from missing-not-at-random feedback. *Advances in Neural Information Processing Systems*, 33:1854–1864, 2020. 3

[50] Chaoyi Wu, Xiaoman Zhang, Ya Zhang, Yanfeng Wang, and Weidi Xie. Pmc-llama: Further finetuning llama on medical papers. *arXiv preprint arXiv:2304.14454*, 2023. 2

[51] Size Wu, Wenwei Zhang, Lumin Xu, Sheng Jin, Wentao Liu, and Chen Change Loy. Clim: Contrastive language-image mosaic for region representation. In *Proceedings of the AAAI Conference on Artificial Intelligence*, pages 6117–6125, 2024. 6, 7

[52] Bin Xie, Jiale Cao, Jin Xie, Fahad Shahbaz Khan, and Yanwei Pang. Sed: A simple encoder-decoder for open-vocabulary semantic segmentation, 2023. 1, 2, 5, 6

[53] Jiarui Xu, Sifei Liu, Arash Vahdat, Wonmin Byeon, Xiaolong Wang, and Shalini De Mello. Open-vocabulary panoptic segmentation with text-to-image diffusion models. In *Proceedings of the IEEE/CVF Conference on Computer Vision and Pattern Recognition*, pages 2955–2966, 2023. 2, 6

[54] Mengde Xu, Zheng Zhang, Fangyun Wei, Yutong Lin, Yue Cao, Han Hu, and Xiang Bai. A simple baseline for open-vocabulary semantic segmentation with pre-trained vision-language model. In *European Conference on Computer Vision*, pages 736–753. Springer, 2022. 2, 6

[55] Mengde Xu, Zheng Zhang, Fangyun Wei, Han Hu, and Xiang Bai. Side adapter network for open-vocabulary semantic segmentation. In *Proceedings of the IEEE/CVF Conference on Computer Vision and Pattern Recognition*, pages 2945–2954, 2023. 1, 2, 6

[56] Qihang Yu, Ju He, Xueqing Deng, Xiaohui Shen, and Liang-Chieh Chen. Convolutions die hard: Open-vocabulary segmentation with single frozen convolutional clip. In *NeurIPS*, 2023. 1, 2, 4, 6

[57] Haotian Zhang, Pengchuan Zhang, Xiaowei Hu, Yen-Chun Chen, Liunian Li, Xiyang Dai, Lijuan Wang, Lu Yuan, Jenq-Neng Hwang, and Jianfeng Gao. Glipv2: Unifying localization and vision-language understanding. *Advances in Neural Information Processing Systems*, 35:36067–36080, 2022. 2

[58] Renrui Zhang, Jiaming Han, Chris Liu, Peng Gao, Aojun Zhou, Xiangfei Hu, Shilin Yan, Pan Lu, Hongsheng Li, and Yu Qiao. Llama-adapter: Efficient fine-tuning of language models with zero-init attention. *arXiv preprint arXiv:2303.16199*, 2023. 2

[59] Bolei Zhou, Hang Zhao, Xavier Puig, Tete Xiao, Sanja Fidler, Adela Barriuso, and Antonio Torralba. Semantic understanding of scenes through the ade20k dataset. *International Journal of Computer Vision*, 127:302–321, 2019. 5, 8

[60] Chong Zhou, Chen Change Loy, and Bo Dai. Extract free dense labels from clip. In *European Conference on Computer Vision*, pages 696–712. Springer, 2022. 2

[61] Kaiyang Zhou, Jingkang Yang, Chen Change Loy, and Ziwei Liu. Conditional prompt learning for vision-language models. In *IEEE/CVF Conference on Computer Vision and Pattern Recognition (CVPR)*, 2022. 2

[62] Kaiyang Zhou, Jingkang Yang, Chen Change Loy, and Ziwei Liu. Learning to prompt for vision-language models. *International Journal of Computer Vision (IJCV)*, 2022. 2

[63] Ziqin Zhou, Yinjie Lei, Bowen Zhang, Lingqiao Liu, and Yifan Liu. Zegclip: Towards adapting clip for zero-shot semantic segmentation. *Proceedings of the IEEE/CVF Conference on Computer Vision and Pattern Recognition (CVPR)*, 2023. 6

[64] Deyao Zhu, Jun Chen, Xiaoqian Shen, Xiang Li, and Mohamed Elhoseiny. Minigpt-4: Enhancing vision-language understanding with advanced large language models. *arXiv preprint arXiv:2304.10592*, 2023. 2

[65] Xiangyang Zhu, Renrui Zhang, Bowei He, Aojun Zhou, Dong Wang, Bin Zhao, and Peng Gao. Not all features matter: Enhancing few-shot clip with adaptive prior refinement. In *Proceedings of the IEEE/CVF International Conference on Computer Vision*, pages 2605–2615, 2023. 2